Fault diagnosis of bearings in multiple working conditions based on adaptive time-varying parameters short-time Fourier synchronous squeeze transform

OPEN ACCESS
IOP Publishing
Measurement Science and Technology
Meas. Sci. Technol. **33** (2022) 124002 (20pp)
https://doi.org/10.1088/1361-6501/ac8abf

Fault diagnosis of bearings in multiple working conditions based on adaptive time-varying parameters short-time Fourier synchronous squeeze transform

Minghui Wei[1,2], Jianwei Yang[1,2,*], Dechen Yao[1,2], Jinhai Wang[1,2] and Zhongshuo Hu[1,2]

[1] School of Mechanical-Electronic and Vehicle Engineering, Beijing University of Civil Engineering and Architecture, Beijing 100044, People's Republic of China
[2] Beijing Key Laboratory of Performance Guarantee on Urban Rail Transit Vehicles, Beijing University of Civil Engineering and Architecture, Beijing 100044, People's Republic of China

E-mail: yangjianwei@bucea.edu.cn

Received 11 June 2022, revised 1 August 2022
Accepted for publication 18 August 2022
Published 7 September 2022

Abstract

Rolling bearings are commonly used components in rotating machinery and play a vital role. When the bearing fails, if it cannot be found and repaired in time, it will cause great economic losses. Time-frequency analysis has been widely used for bearing fault signals under non-stationary operating conditions, but the existing methods have problems such as poor adaptability under multiple operating conditions. At the same time, the low time-frequency resolution and poor energy aggregation also affect the fault feature extraction effect. Aiming at these problems, this paper proposes a bearing fault detection method, which combines empirical mode decomposition and adaptive time-varying parameter short-time Fourier synchronous squeezing transform (AFSST), it solves the problem of adapting to signals under multiple operating conditions; A weighted least squares estimation time-varying parameter algorithm is proposed, which improves the calculation speed by 29% under the premise of ensuring the calculation accuracy; A time-varying index of energy effective compression ratio is proposed to accurately measure the time-varying energy aggregation of time-frequency analysis methods. Using short-time Fourier transform, continuous wavelet transform, wavelet synchrosqueezed transform, and AFSST to analyze the simulated FM signal, the results show that the AFSST transform has better time-frequency resolution and higher energy-efficient compression rate globally. Through the verification of the fault experimental data of rolling bearings, the diagnosis method proposed in this paper can accurately extract the bearing fault characteristics, has a good diagnosis ability in the multi-working operating environment, and has strong robustness and anti-noise interference.

* Author to whom any correspondence should be addressed.

Keywords: AFSST, time-varying parameters, weighted least squares estimation, energy effective compression ratio, fault diagnosis

(Some figures may appear in colour only in the online journal)

1. Introduction

Bearings are widely used in various types of rotating machinery, and it is difficult to avoid the resulting component or system failure [1]. Bearing faults will produce shock features in the vibration signal during operation, and the judgment of the operating state can be realized by identifying the shock features [2]. However, the operating conditions of rotating machinery are complex, working under the condition of speed change and load, and the bearing fault signal and noise are aliased, so the bearing vibration signal has obvious non-stationary and time-varying characteristics [3]. Simple spectrum analysis methods for stationary signals can no longer be applied directly, Time-frequency analysis methods are very effective tools for dealing with non-stationary signals [4].

At present, many scholars have conducted research on time-frequency analysis methods [5] and achieved fruitful results [6]. Tang *et al* [7] proposed a composite fault diagnosis strategy based on the classification of multiple time-frequency curves, matching the average ratio between the curves of interest with the theoretical fault characteristic coefficients to determine the fault type. Tiwari and Upadhyay [8] propose a novel self-adaptive signal decomposition technique: concealed component decomposition, which was validated on experimental datasets. Wei *et al* [9] proposed a time-varying envelope filtering method to extract the weak fault features of the space-bearing cage and improve the signal-to-noise ratio of the original vibration signal. Xu *et al* [10] proposed the match-extracting chirplet transform to analyze multi-component dynamic signals. The experiments proved that it has good performance in time-frequency localization and noise robustness. Chen *et al* [11] proposed a fault pulse extraction and feature enhancement method for bearing fault diagnosis, which enhanced the extraction of weak transient features. Shi *et al* [12] proposed an instantaneous frequency synchronous generalized stepwise demodulation transformation method for time-frequency analysis of non-stationary vibration signals. Yu [13] proposed a high-resolution time-frequency analysis method for analyzing strong non-stationary signals, which provides better performance in handling strong non-stationary signals and signals with added noise. Liu *et al* [14] proposed a time-frequency processing method called synchro-squeeze extraction transform, which can well extract the time-varying information of non-stationary signals and has better noise robustness. Ma *et al* [15] proposed a method to extract the main components from time-frequency images, which realized the bearing fault diagnosis under variable working conditions. Hu *et al* [16] proposed an adaptive time-domain signal segmentation method, which divides long-term non-steady-state signals into multiple short-term steady-state signals, which can effectively suppress the high-amplitude components of the vibration signal of subway gearboxes. Xu *et al* [17] proposed generalized S-simultaneous extrusion to extract variation, a new time-frequency post-processing algorithm with good noise robustness. Wang *et al* [18] proposed an ensemble decision method that combines a dislocation time-frequency representation and a pre-trained convolutional neural network to evaluate gear health status. He *et al* [19] proposed a modified deep autoencoder driven by a multi-source parameter, which confirmed the feasibility of cross-domain fault prediction. Han *et al* [20] proposed a new multi-compression method based on wavelet transform to accurately extract fault-related features and used second-order instantaneous frequency estimation to approximate the real intermediate frequency of the analyzed signal. Multi-resolution high-quality time-frequency representation of non-stationary signals at intermediate frequencies. Shao *et al* [21] proposed a new fault diagnosis method for variable-speed rotor bearing systems based on two-stage parameter transfer and infrared image, and realized the extended use of the diagnosis model. Lee *et al* [22] proposed a time-frequency envelope analysis to overcome the influence of impulse noise, which can be performed by dividing the signal into several parts through a time window, which can eliminate the influence of impulse noise. He *et al* [23] proposed an enhanced depth transfer autoencoder for fault diagnosis of bearings installed on different machines. Li *et al* [24] proposed a fusion framework based on the confidence weight support matrix machine, and the experiment proved that the method has good fault diagnosis performance. Deng *et al* [25] proposed a bearing fault detection method based on hybrid singular value decomposition (SVD) denoising and adaptive time redistribution transformation. The experimental results show that the algorithm has better performance in extracting weak bearing fault features in a strong background noise environment. Lv *et al* [26] proposed a time-frequency analysis method of longitudinally synchronous compression change, which preserves the ability of pattern extraction and reconstruction, and can accurately characterize the fast event characteristics of the signal within a large window size. Lin *et al* [27] proposed an optimal weighted sliding window signal segmentation algorithm based on the second-order synchronous compression S-transform, which can improve the spectrum aggregation of the signal and obtain high-precision signal instantaneous frequency (IF) estimation in the low signal-to noise ratio (SNR) environment. Meng *et al* [28] used the empirical modal decomposition algorithm to extract the features of rolling bearings and realize the fault classification of rolling bearings. Bai *et al* [29] proposed a new spectral Markov transition field algorithm to represent the spectral characteristics of vibration signals in the form of

images. To improve the separation effect of short-time Fourier transform (STFT) for multi-components, Li *et al* [30] proposed good separation conditions and established an FSST with adaptive time-varying parameters, which improved the time-frequency resolution.

Many scholars have made many attempts to improve the time-frequency resolution and anti-interference performance, but these methods have certain limitations. Some time-frequency processing effects are affected by the selection of convolution kernels, and there may be large differences; the selection of some windows does not have global adaptation, and only selects the frequency that is suitable for the strongest separation energy. These processing algorithms have great constraints on the practical application of non-stationary signals.

Aiming at these problems, this paper proposes a new diagnostic strategy. The original signal is decomposed by empirical mode decomposition (EMD), the intrinsic mode function (IMF) with a higher correlation coefficient is selected for signal reconstruction, the signal irrelevant to the fault feature is filtered out, the shock feature is extracted by envelope demodulation, and the window prediction interpolation algorithm is proposed to realize the fast window width parameter. To determine, time-frequency analysis of the reconstructed signal was performed using adaptive short-time Fourier synchronized squeeze transform (AFSST). It realizes the analysis and diagnosis of complex fault signals. Compared with STFT, continuous wavelet transform (CWT) and wavelet synchrosqueezd transform, it shows that AFSST has better time-frequency resolution and frequency resolution, has strong self-adaptation, and can obtain higher frequency resolution at a lower sampling rate, Moreover, it has strong anti-interference performance and can be used for bearing fault diagnosis under actual working conditions.

The work of this paper is organized as follows: The second Section introduces the EMD algorithm and the adaptive short-time Fourier synchronous squeezing transform, proposes a time-varying parameter prediction interpolation algorithm, and defines the energy-efficient compression ratio. The third section uses the simulation signal to verify the diagnostic algorithm proposed in this paper. The fourth section analyzes four experimental fault signals with the algorithm proposed in this paper, and compares the results with STFT, CWT and WSST. The fifth section is the conclusion of this paper.

2. EMD and time-varying parameter short-time Fourier synchronous extrusion transform

2.1. Principles of EMD

The EMD method is an adaptive analysis method, it performs adaptive time-frequency decomposition according to the local time-varying characteristics of the signal, which eliminates human factors and overcomes the defect of traditional methods that use meaningless harmonic components to represent non-stationary nonlinear signals, suitable for the analysis of non-stationary nonlinear signals [31]. For a vibration signal $x(t)$, the EMD decomposition algorithm is as follows:

(a) Use the cubic spline interpolation curve to connect the maximum and minimum points of the signal $x(t)$ to be processed, so that the signal is surrounded by it, and the sequence consisting of the mean value of the upper and lower envelopes is $m(t)$.

(b) Subtract $m(t)$ from $x(t)$, and check whether the obtained cc h_1 satisfies the condition of the fundamental mode component. If so, it is regarded as the first fundamental mode component; otherwise, the calculation of formula 1 is repeated until the condition is met

$$\begin{aligned} h_1 &= x(t) - m(t) \\ c_1(t) &= h_1(t). \end{aligned} \tag{1}$$

(c) Subtract the first fundamental mode component $c_1(t)$ from the original signal to obtain the residual sequence $r_1(t)$

$$r_1(t) = x(t) - c_1(t). \tag{2}$$

(d) The above operation is repeated with the $r_1(t)$ obtained in step 3 as the 'original' signal, and other basic mode components are obtained in sequence, and the processing is stopped after the preset conditions are met.

The original signal $x(t)$ can be expressed as the sum of several fundamental mode components and a remainder:

$$x(t) = \sum_{n}^{i=1} c_i(t) + r_n(t). \tag{3}$$

2.2. Selection of IMF components

EMD can decompose the original signal into multiple IMF components, but there will be false components and trend components unrelated to faults in the components. By eliminating these components, the anti-interference performance in the subsequent time-frequency processing can be improved. The correlation coefficient r_k can be used to measure the degree of correlation between the IMF component and the original signal. The greater the correlation, the more fault features are included. The choice can be made by the size of the correlation coefficient. The formula for calculating the correlation coefficient is:

$$r_K = \frac{\sum_{i=1}^{n} \left(R_{\mathrm{IMF}K}(i) - \bar{R}_{\mathrm{IMF}K}\right)\left(R_X(i) - \bar{R}_X\right)}{\left\{\sum_{i=1}^{n} \left(R_{\mathrm{IMF}K}(i) - \bar{R}_{\mathrm{IMF}K}\right)^2 \sum_{i=1}^{n} \left(R_X(i) - \bar{R}_X\right)^2\right\}^{1/2}}. \tag{4}$$

In the formula, n is the number of sample samples; R_x and $R_{\mathrm{IMF}K}$ are the samples of the original signal and each eigenmode function, respectively, $\bar{R}_{\mathrm{IMF}K} = \sum_{i=1}^{n} R_{\mathrm{IMF}K}(i)/n$, K is the number of IMF components.

2.3. Time-varying parameter FSST and good separation conditions

Most of the current FSST algorithms are based on fixed-window STFT, which determines that high time resolution

and frequency resolution cannot be obtained at the same time. For the signal $x(t) \in L_2(\mathbb{R})$, this paper considers the STFT with time-varying parameters $\sigma(t)$, and its signal definition expression is:

$$\begin{aligned}\tilde{V}_x(t,\eta) &:= \int_{-\infty}^{\infty} x(\tau)\, g_{\sigma(t)}(\tau - t)\, e^{-i2\pi\eta(\tau - t)} \mathrm{d}\tau \\ &= \int_{-\infty}^{\infty} x(t+\tau)\, \frac{1}{\sigma(t)} g\left(\frac{\tau}{\sigma(t)}\right) e^{-i2\pi\eta\tau} \mathrm{d}\tau. \end{aligned} \quad (5)$$

Here $g_{\sigma(t)}(\tau)$ is the window function, $\sigma = \sigma(t)$ is a positive function of t, and $g_{\sigma(t)}(\tau)$ is defined as

$$g_{\sigma(t)}(\tau) := \frac{1}{\sigma(t)} g\left(\frac{\tau}{\sigma(t)}\right). \quad (6)$$

Here $g \in L_2(\mathbb{R})$. The window width of $g_{\sigma(t)}(\tau)$ is $\sigma(t)$, depending on the time variable t

$$g_\sigma(t) = \frac{1}{\sigma} g\left(\frac{t}{\sigma}\right) \quad (7)$$

where the parameter $\sigma > 0$, $g(t)$ is a positive function in $L_2(\mathbb{R})$, and $g(0) \neq 0$, it has a certain decay order when in $t \to \infty$. If

$$g(t) = \frac{1}{\sqrt{2\pi}} e^{-\frac{t^2}{2}}. \quad (8)$$

Here $g_\sigma(t)$ is a Gaussian window function. When $\tilde{V}_x(t,\eta) \neq 0$ in (t,η), the phase transition $\omega_x^{adp}(t,\eta)$ can be expressed as:

$$\begin{aligned}\omega_x^{adp}(t,\eta) = \mathrm{Re}\left\{\frac{\partial_t\left(\tilde{V}_x(t,\eta)\right)}{i2\pi\tilde{V}_x(t,\eta)}\right\} + \frac{\sigma'(t)}{\sigma(t)}\mathrm{Re}\left\{\frac{\tilde{V}_x^{\tau g'(\tau)}(t,\eta)}{i2\pi\tilde{V}_x(t,\eta)}\right\}, \\ \text{for } \tilde{V}_x(t,\eta) \neq 0. \end{aligned} \quad (9)$$

Then the FSST of the time-varying parameter is defined as

$$R_x^{adp}(t,\xi) := \int_{\left\{\eta\in\mathbb{R}:\tilde{V}_x(t,\eta)\neq 0\right\}} \tilde{V}_x(t,\eta)\delta\left(\omega_x^{adp}(t,\eta) - \xi\right)\mathrm{d}\eta. \quad (10)$$

Let $x(t) = \sum_{k=1}^{k} x_k(t)$, where each $x(t) = A_k e^{i2\pi\phi_k(t)}$ is a chirp, and $\phi'_{k-1}(t) < \phi'_k$. If

$$4\alpha\sqrt{\pi}\sqrt{\left|\phi_k''(t)\right| + \left|\phi_{k-1}''(t)\right|} \leqslant \phi_k'(t) - \phi_{k-1}'(t), \quad k = 2,\ldots,K \quad (11)$$

$$\begin{aligned}&\max_{2\leqslant k\leqslant K}\left\{\frac{4\alpha}{b_k(t) + \sqrt{b_k(t)^2 - 8\alpha a_k(t)}}\right\} \\ &\leqslant \min_{2\leqslant k\leqslant K}\left\{\frac{4\alpha}{b_k(t) - \sqrt{b_k(t)^2 - 8\alpha a_k(t)}}\right\}. \end{aligned} \quad (12)$$

In the formula,

$$\begin{aligned} a_k(t) &= 2\pi\alpha\left(\left|\phi_{k-1}''(t)\right| + \left|\phi_k''(t)\right|\right) \\ b_k(t) &= \phi_k'(t) - \phi_{k-1}'(t) \\ \alpha &= \frac{1}{2\pi}\sqrt{2\ln(1/\in)}. \end{aligned}$$

For a multi-component signal $x(t)$, we call equations (11) and (12) as good separation conditions based on the linear-frequency modulation (LFM) model. Any on both sides of inequality 12 can separate the components in the time-frequency plane. As mentioned above, we should choose as small as possible, since a smaller $\sigma(t)$ can get a sharper synchro-squeeze effect. Therefore, we propose that σ is determined by $\sigma(t)$ based on the LFM model:

$$\sigma(t) = \max\left\{\frac{4\alpha}{b_k(t) + \sqrt{b_k(t)^2 - 8\alpha a_k(t)}} : 2 \leqslant k \leqslant K\right\}. \quad (13)$$

2.4. Time-varying parameter prediction and interpolation algorithm

With the good separation conditions mentioned in the previous section, a time-varying parameter $\sigma(t)$ that changes with time and has a sharper frequency expression can be obtained for non-stationary signals, and we can obtain better time resolution and frequency resolution. However, the determination of suitable time-varying parameters requires a lot of search calculations, which greatly affects the efficiency of the algorithm. In order to optimize this problem, this paper proposes a weighted least squares prediction and interpolation algorithm, which realizes that the global time-varying parameters of the signal can be determined with fewer calculation times, and the calculation time is greatly reduced.

The state of a non-stationary signal at a certain moment will be affected by the previous period of time, and will also affect the next period of time, but the impact size will change accordingly with the change of the time parameter. In order to avoid the time parameter from affecting the prediction accuracy, The weighted least squares method is introduced for fitting estimation. The time-varying parameters calculated using the separation conditions are used as anchor points, and different weighting coefficients are selected in the least squares estimation according to the time distance between the position of each anchor point and the prediction point, so as to improve the prediction accuracy of the time-varying parameters. The coefficients are estimated by minimizing the generalized residual sum of squares, which can be expressed as:

$$\begin{aligned}\mathrm{RSS}\ (\beta) &= (Y - X\beta)^{\mathrm{T}} W (Y - X\beta) \\ W &= \begin{pmatrix} \frac{1}{w_1} & \cdots & 0 \\ \vdots & \ddots & \vdots \\ 0 & \cdots & \frac{1}{w_i} \end{pmatrix}. \end{aligned} \quad (14)$$

The formula, W represents the weight matrix. Then the weighted least squares estimation can be solved as follows:

$$\beta = \left(X^{\mathrm{T}}WX\right)^{-1}X^{\mathrm{T}}WY. \tag{15}$$

During window length prediction, six adjacent anchor points are selected as the fitting data points before and after the prediction point, and the weighting coefficient matrix [0.2, 0.35, 0.8, 0.8, 0.35, 0.2] is selected according to the time parameter. The weighted least squares estimation is used to fit the data, and then the time-varying parameters of the prediction points are obtained according to the fitting results, so as to quickly determine the window length.

Algorithm calculation steps:

Let $\sigma_i, i = 1,2,\ldots,n$ be the time-varying parameter to be determined, and the signal $S(t), t = t_1, t_2, \ldots, t_n$ to be processed.

Step 1: Set $t = t_1, t_2, t_3, t_5, t_7, t_9$, use good separation conditions to determine $\sigma_1, \sigma_2, \sigma_3, \sigma_5, \sigma_7, \sigma_9$;

Step 2: Use the obtained 6 points as anchor points to fit using the weighted least squares method;

Step 3: Use the fitting function to predict the central time-varying parameter $\sigma_i, i = 4,6,\ldots,n-3$;

Step 4: Calculate the new time-varying parameter to determine whether it is the last data point. If yes, go to step five. If not, update the data anchor point and jump to step 2;

Step 5: To ensure good global coherence, use a low-pass filter $B(t)$ to smooth the time-varying parameters σ_i to obtain the time-varying parameters: $\sigma_e(t) = (C * B)(t)$.

2.5. Energy effective compression ratio

Through the time-frequency processing method, the time-frequency signal is converted into a time-frequency graph, so as to better feature expression and fault judgement. However, affected by interference factors such as invalid signals and background noise, the characterization effect of the time-frequency graph may not be ideal. At present, many scholars use Rényi entropy as a measure of the time-frequency aggregation effect, and improve the time-frequency processing method. The determination of the time-varying parameters in this paper is more input research based on it. In order to better highlight the improvement of the time-frequency aggregation effect of AFSST, this paper proposes the energy effective compression ratio parameter (EECR) to measure the time-frequency processing effect qualitatively.

The obtained time-frequency diagram is divided according to the time scale, and the frequency component with the strongest energy at a certain time is extracted as the effective energy, and the rest of the divergent energy is mostly noise energy or fault energy that cannot be extracted. The ratio is defined as the effective compression ratio of energy, the dynamic relationship between the effective compression ratio and time can be obtained, and the effect of different

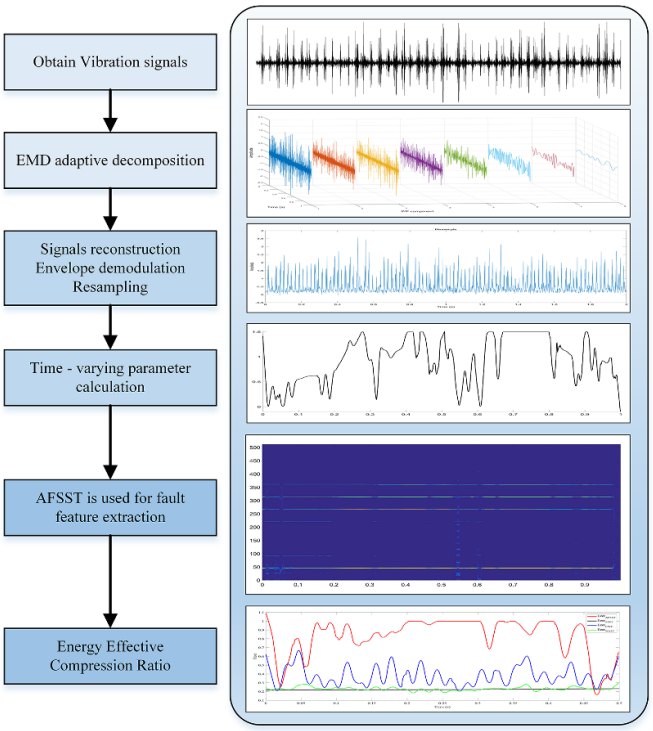

Figure 1. Signal processing flowchart.

time-frequency analysis methods can be accurately measured. The calculation formula is as equation (16):

$$\mathrm{Ecre}_t = \frac{\sum_{i=0}^{k} y_{(\mathrm{t,i})}}{\sum_{i=0}^{m} x_{(\mathrm{t,i})}} \quad (\mathrm{t} = 1,2,\ldots,n). \tag{16}$$

In the formula: n is the number of time dimensions, m is the number of frequency dimensions, k is the number of statistical effective energy, $y_{t,i}$ is the effective energy matrix, and $x_{t,i}$ is the total energy matrix. According to the signal components in this paper, the number of statistics k is set to 5.

2.6. Signal processing flow

For the fault feature identification of non-stationary signals, based on the above research, this paper proposes a new signal diagnosis strategy, as shown in figure 1:

3. Simulation signal analysis

In order to verify the effectiveness of the AFSST algorithm for non-stationary signals, a simulated signal $X(t)$ of frequency modulation and amplitude modulation is established, and the AFSST algorithm proposed in this paper is used for processing, and the results are compared with STFT, CWT and WSST.

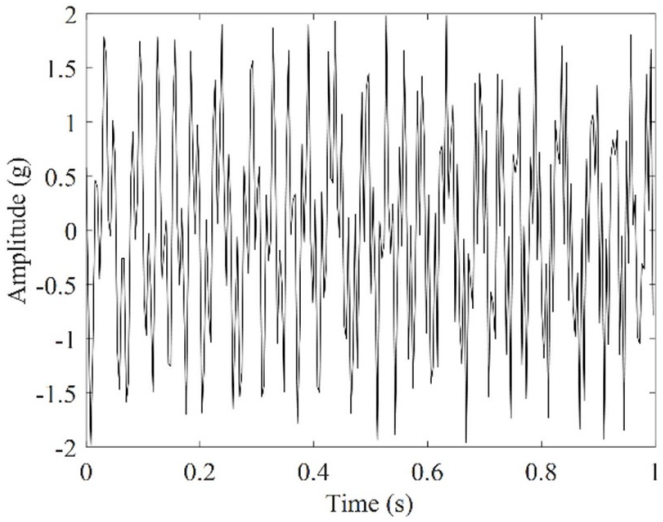

Figure 2. Time domain waveform.

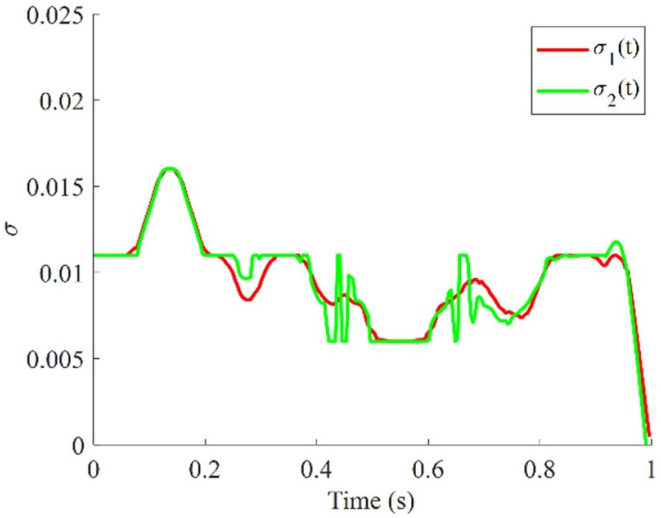

Figure 3. Time-varying parameter σ.

3.1. FM signal

The simulated signal is composed of two cosine frequency modulated (FM) signals of different frequencies superimposed:

$$\begin{cases} x_1(t) = \cos(2\pi \times 25t + \cos(10\pi t)) \\ x_2(t) = \cos(2\pi(60t + 30t^2)) \\ x(t) = x_1(t) + x_2(t) \end{cases} . \quad (17)$$

In the formula, $x_1(t)$ is the cosine FM signal whose frequency is oscillating at 25 Hz; $x_2(t)$ is the chirp signal whose initial frequency is 60 Hz. Set the sampling time to one second and the sampling frequency to Fs = 256 Hz.

The time domain diagram of the simulated signal is shown in figure 2. Figure 3 shows different time-varying parameters σ of the simulated signal, σ_1 which are the time-varying parameters calculated by using the weighted least squares fitting prediction, and σ_2 are the time-varying parameters calculated globally. In order to qualitatively measure the fitting degree, the goodness-of-fit parameter is used to evaluate the fitting effect. The statistic to measure the goodness of fit is the coefficient of determination R^2. The maximum value of R^2 is 1. The closer the value of R^2 is to 1, the better the fit of the regression line to the observations. It can be seen that when the goodness of fit is 0.9064, the calculation speed of time-varying parameters is increased by 29%, and the calculation efficiency is greatly improved. The specific parameters are shown in table 1.

Use AFSST transform, STFT transform, CWT transform and WSST transform to perform time-frequency transform on the simulated signal, and the time-frequency diagram is obtained as shown in figure 4. It can be seen that the STFT transform can separate the two frequency components, but the frequency resolution is low. For the cosine frequency modulation component, there is a serious energy dispersion phenomenon, and the frequency components cannot be identified; the CWT transform can clearly separate the two types of frequency modulation components, but CWT has serious energy dispersion in the high-frequency part, and cannot accurately locate the frequency components in the low-frequency region. WSST can clearly separate the two FM components, and accurately gather energy for the chirp components, however, for the cosine FM signal, serious energy leakage occurs, and the time resolution and frequency resolution are not ideal. AFSST can clearly separate two FM signals, and can accurately squeeze energy for cosine FM components, which has obvious advantages in time resolution and frequency resolution.

Figure 5 shows the EECR parameters. It can be seen that AFSST has a better effective energy compression rate globally, which greatly exceeds other processing methods, which proves that the diagnostic method can achieve effective energy accumulation.

3.2. Noise-added FM signal

In order to verify the anti-interference performance of the AFSST algorithm for noise, on the basis of the above cosine FM signal, random white Gaussian noise with a mean of 0 and a standard deviation of 0.5 is added. The time-domain waveform is shown in figure 6, and the time-varying parameters are shown in figure 7.

Using AFSST, STFT, CWT and WSST time-frequency algorithms for analysis, the time-frequency diagrams obtained are shown in figure 8. Both STFT and CWT are interfered with by noise, and different levels of interference frequencies appear, which affect the determination of actual frequency components and energy accumulation. WSST basically realizes the separation of the chirp signal, but still produces serious energy dispersion near the cosine frequency component, and the time resolution and frequency resolution are poor. AFSST can better separate two different frequency modulation components, has good time resolution and frequency resolution, basically does not have large interference frequencies, and has strong anti-interference performance.

The EECR under the noise-added signal is shown in figure 9. Compared with the un-noised signal, the EECR as

Table 1. Calculation parameters of time-varying parameter σ.

Category	Global calculation	Predictive Imputation Algorithms	Speed boost	Goodness of fit
Index	7.361 s	5.279 s	29%	0.9064

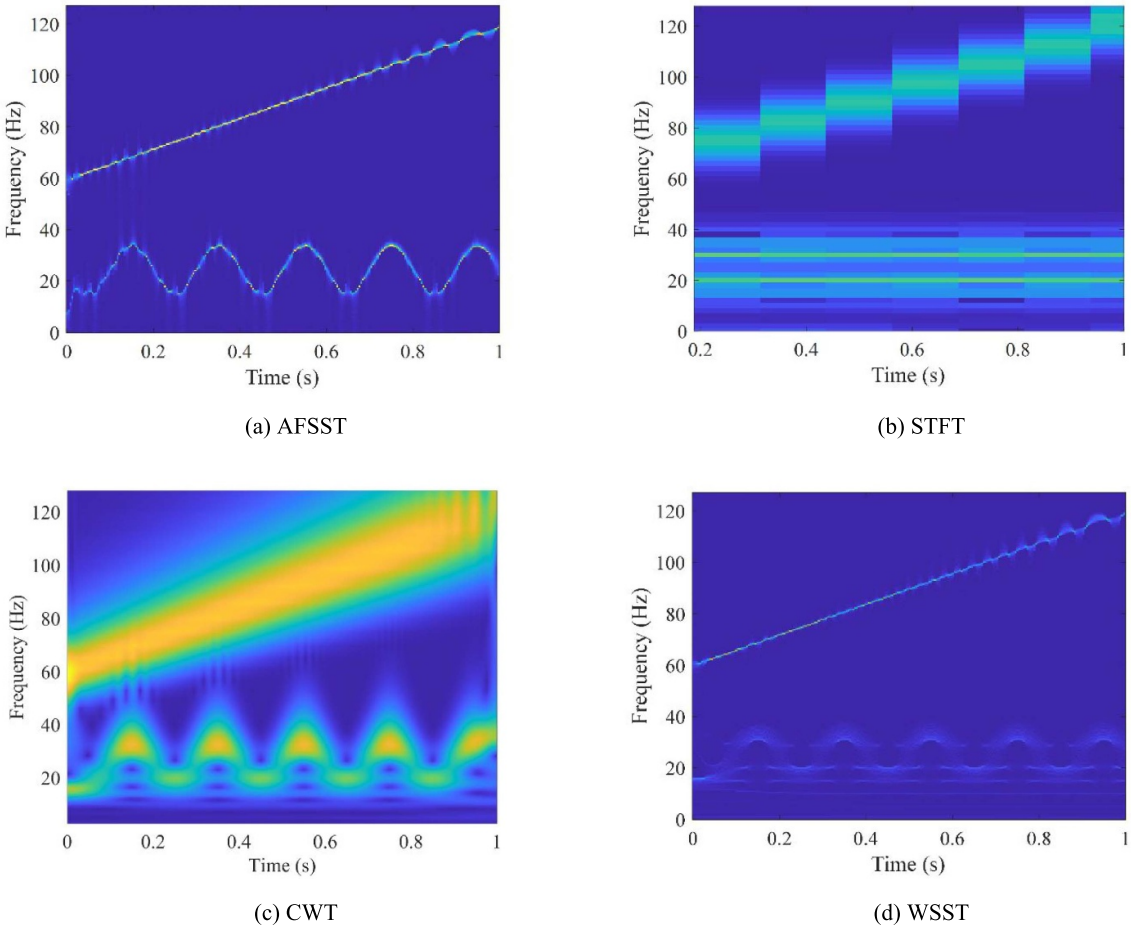

Figure 4. Time-frequency analysis.

a whole has a certain decrease, which also shows the rationality of the EECR parameter. However, compared with several other methods, AFSST has a higher effective energy compression rate globally, which proves that the AFSST method has good anti-interference performance and feature extraction ability.

4. Test verification

4.1. Data of western reserve university

In order to further verify the validity and accuracy of the diagnostic algorithm proposed in this paper, the public data set of the bearing data test bench of Case Western Reserve University was analyzed and diagnosed [32], the test bench is shown in figure 10. The test bearing is a 6205-2RS JEM SKF deep groove ball bearing at the drive end. The specific parameters are shown in table 2.

The pit damage with a diameter of 0.1778 mm and a depth of 0.2794 mm was machined on the inner raceway of the bearing with an electric spark to simulate a single point failure. The acquisition parameters of the experimental data are: the rotational speed is 1797 r min^{-1}, the available frequency is $f_\text{r} = 29.95$ Hz, and the sampling frequency is 12 kHz. According to the basic parameters of the bearing and the rotational frequency of the motor, the fault characteristic frequency (FCF) of the inner ring of the bearing and the fault frequency of the outer ring of the bearing can be calculated by equation (18).

$$f_0 = \frac{Z}{2}\left(1 - \frac{d}{D}\cos\theta\right) f_\text{r} = 3.5848 f_\text{r}$$

$$f_i = \frac{Z}{2}\left(1 + \frac{d}{D}\cos\theta\right) f_\text{r} = 5.4152 f_\text{r}. \tag{18}$$

In the formula, Z is the number of rolling elements; d is the diameter of the rolling elements; D is the diameter of the pitch

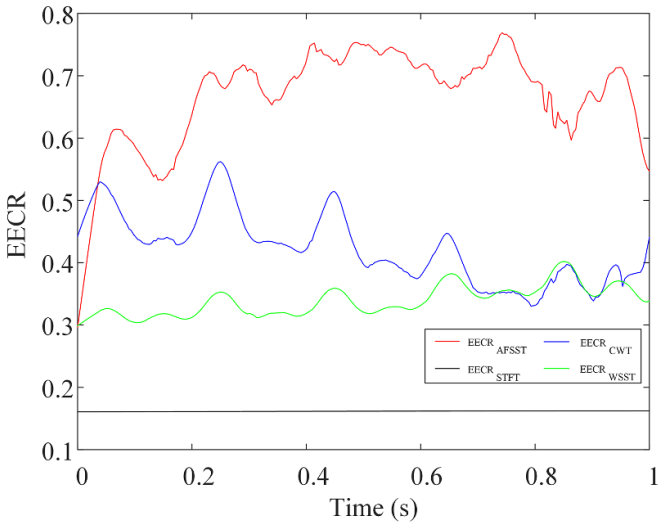

Figure 5. EECR.

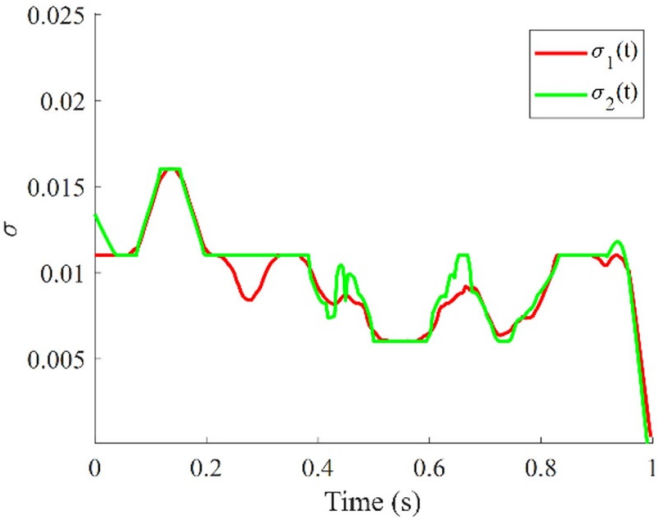

Figure 7. Noise time-varying parameter σ.

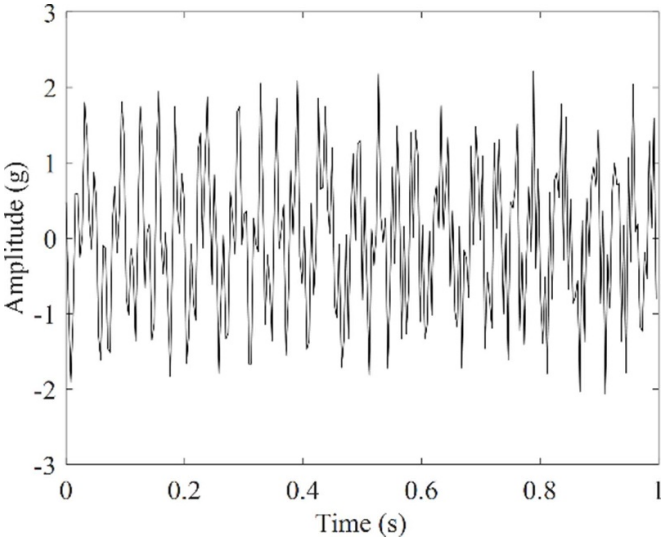

Figure 6. Noise-added time-domain waveform.

circle; θ is the pressure angle. $f_i = 162.18$ Hz can be obtained through the parameters of the bearing.

Taking the data of length 1S, the time domain signal of the faulty bearing is shown in figure 11. For analyzing the spectrum of 0 Hz–512 Hz, figure 12 shows the fast Fourier transform (FFT) spectrum of the selected data. It can be seen that there is a higher amplitude near 162.6 HZ, which proves that this frequency may be the fault frequency of the inner ring of the bearing. Figure 13 shows the time-varying parameters. Then perform AFSST, STFT, CWT, and WSST analysis on the fault vibration signal.

Figure 14 shows the time-frequency processing results. The FCF of 162 Hz can be accurately located by AFSST, and under the optimization of time-varying parameters, it has a good frequency resolution in the whole world, showing good anti-interference performance. Using STFT, the energy of the fault frequency band can be seen, but due to the interference of noise, the energy is relatively divergent, the fault characteristics and interference signals cannot be accurately separated, and the frequency resolution is poor. The FCF can also be seen through CWT and WSST, but the characteristic frequency band obtained by CWT is too wide, and the FCF cannot be clearly located; while WSST transform solves the problem of CWT energy divergence, and has good energy aggregation, but the aggregated characteristic energy band diverges in a cosine shape, which has a large error with the actual FCF, and the frequency resolution is not accurate enough.

Figure 15 shows the change of EECR. It can be seen that the use of synchronous extrusion can improve the energy concentration, while STFT and CWT have weak energy concentration, which is not conducive to the resolution of features. WSST has good energy aggregation, but the frequency resolution is not enough to accurately locate the fault frequency. AFSST performs well in terms of effective energy concentration rate and also has excellent frequency resolution. Through the analysis and verification of the actual bearing data set, it is verified that AFSST has a certain anti-interference performance, can accurately locate the FCF, and has good time-frequency resolution and good frequency resolution.

4.2. University of ottawa data

The variable speed data from the University of Ottawa is used to verify the bearing diagnosis algorithm proposed in this paper [33]. The experiments are carried out on the Spectra-Quest mechanical fault simulator (MFS-PK5M). The experimental setup is shown in figure 16. The motor drives the shaft, and the rotational speed is controlled by an AC drive. The accelerometer is installed on the experimental bearing housing, and an incremental encoder is used to measure the rotational speed. Two ER16K rolling bearings are installed to support the shaft, the healthy bearing on the left and the experimental bearing on the right.

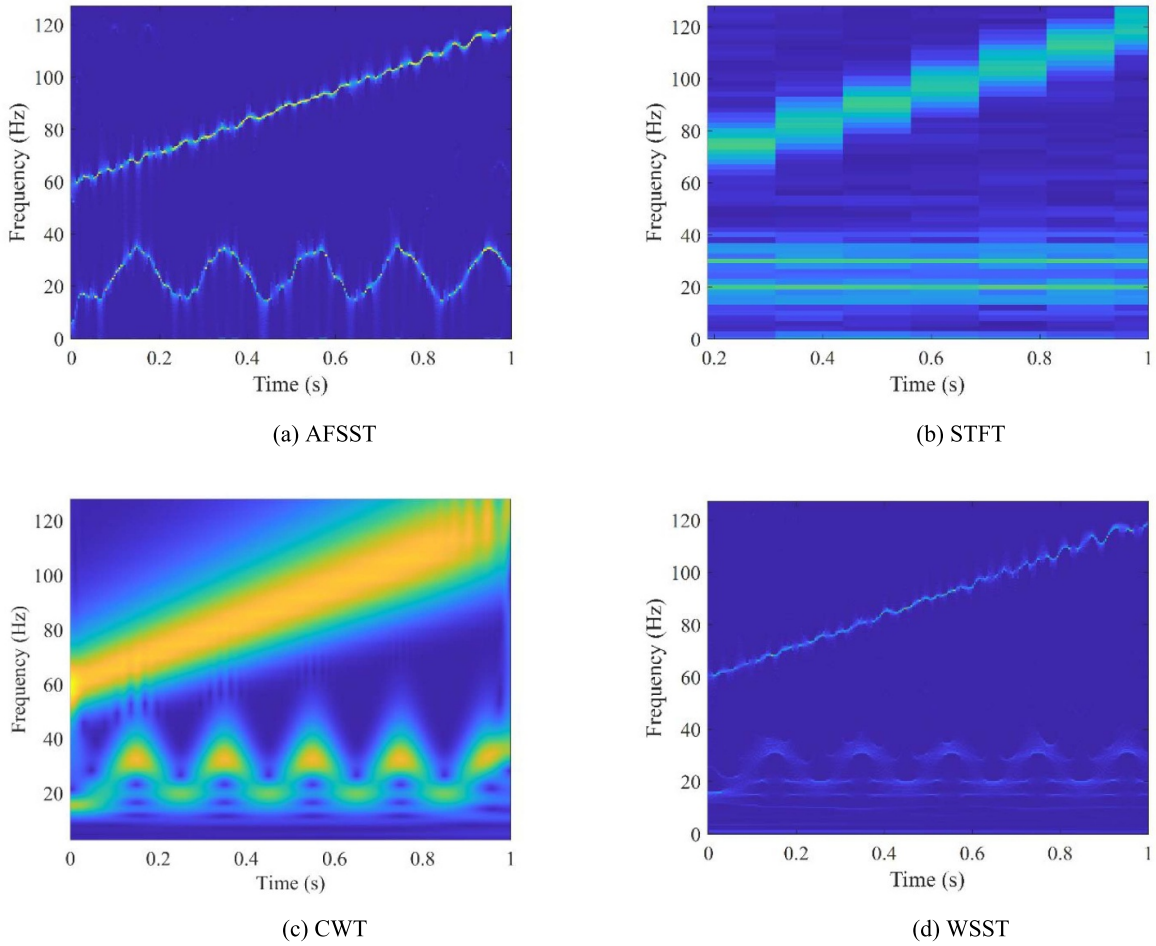

Figure 8. Time-frequency analysis.

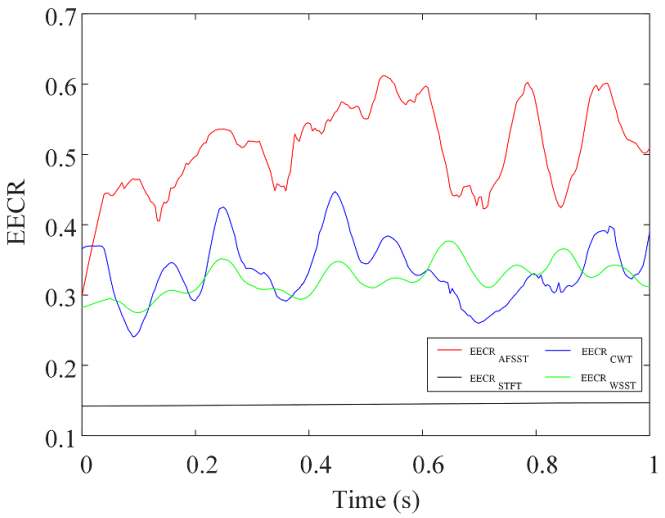

Figure 9. EECR.

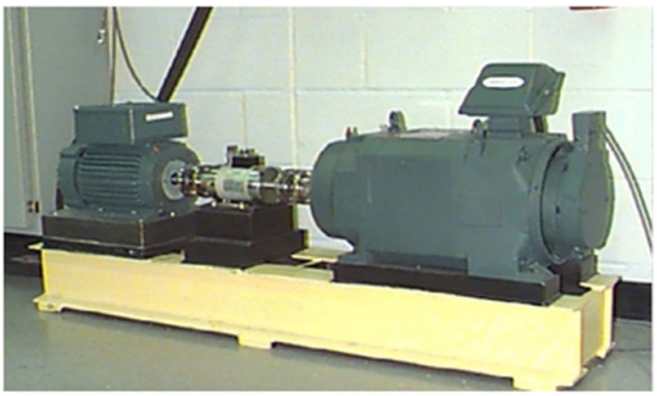

Figure 10. Western reserve university test bed.

By observing the FCF in the frequency domain, it is possible to detect and diagnose bearing faults. Table 3 gives the structural parameters of the bearing in the experiment. According to the bearing parameters, the FCF coefficient of the inner ring of the bearing can be calculated by the above formula to be 5.43, that is, the characteristic frequency of the inner ring of the bearing is BPFI $= 5.43 f_r$. The first second data of the inner ring fault data I-A-1 is selected for analysis, the rotation speed is increased from 12.5 Hz to 14.03 Hz, and the fault frequency is increased from 66.75 Hz to 74.9 Hz.

The time domain diagram is shown in figures 17 and 18 is the time-varying parameters.

Table 2. Bearing parameters.

Inner ring diameter	Outer ring diameter	Roller diameter	Pitch diameter	Number of the rolling	Contact angle
25 mm	52 mm	7.94 mm	39.04 mm	9	0°

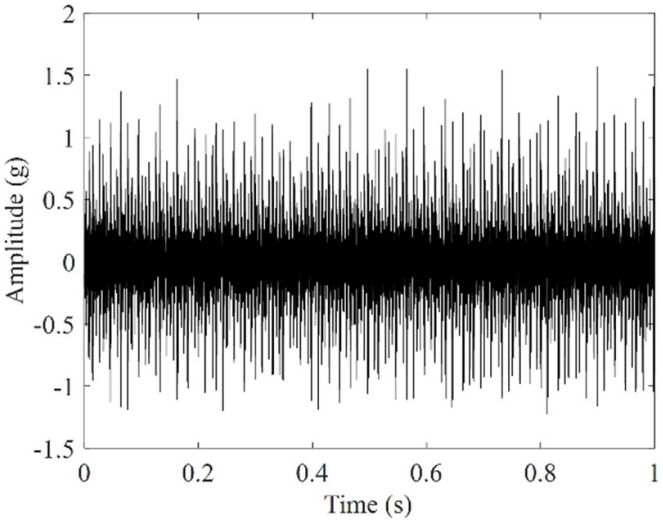

Figure 11. Time domain waveform.

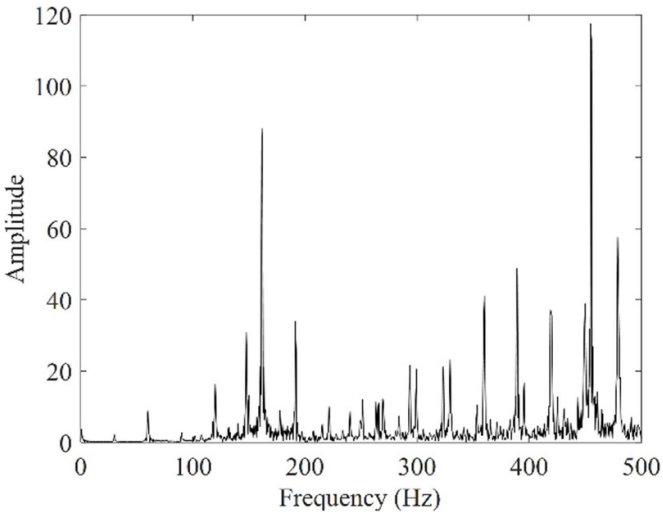

Figure 12. Spectrum analysis.

Using four time-frequency processing methods such as AFSST, STFT, CWT, and WSST, the time-frequency diagrams are obtained as shown in figure 19. The time-frequency diagram obtained by the AFSST method can see the obvious fault time-frequency curve, Accurate energy accumulation has been carried out for the fault characteristics of the one-fold frequency and the double-frequency frequency, and the frequency identification is also relatively accurate, and no frequency appears Offset, the frequency components of triple frequency can be seen in some areas, which has a good filtering effect on background noise and interference frequency

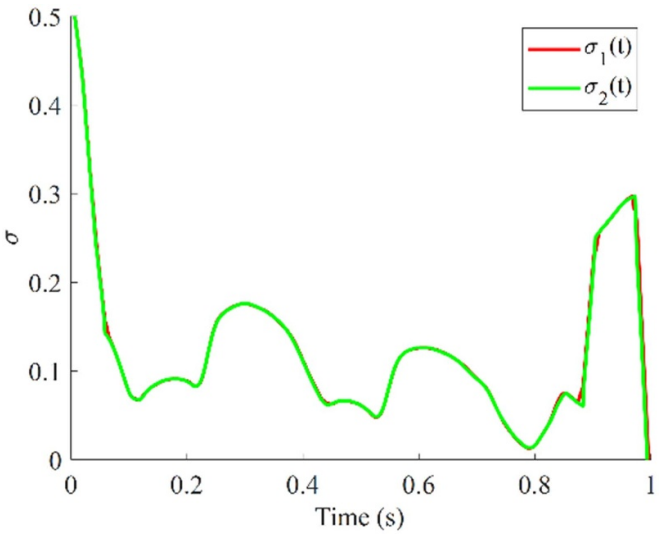

Figure 13. Time-varying parameter σ.

components. The time-frequency diagram obtained by the STFT method can see three faint fault frequency bands, and the frequencies are more spread out, it is difficult to determine the frequency center, and the suppression of background noise and interference frequencies is not ideal, which seriously affects the extraction and resolution of fault features; the time-frequency diagram obtained by CWT and WSST has poor extraction effect on fault features, and the frequency energy is too Dispersed, and mixed with background noise and interference frequencies, the extraction of fault features cannot be achieved.

The EECR parameters are shown in figure 20. Compared with the other three time-frequency processing methods, the overall effective energy compression rate of the AFSST algorithm is significantly higher than the other three algorithms. It is proved that AFSST has great advantages in energy aggregation, and can accurately extract fault features in bearing vibration signals and filter interference signals.

4.3. Experimental platform construction and signal acquisition

Build the bearing fault test platform by yourself to collect the measured data, and verify the algorithm proposed in this paper based on the measured data. The basic transmission diagnosis simulator produced by SpectraQuest Company in the United States is used as the bearing simulation test bench. The test bench can realize different assembly methods and parts selection, to simulate various working conditions. The experimental platform is shown in figure 21.

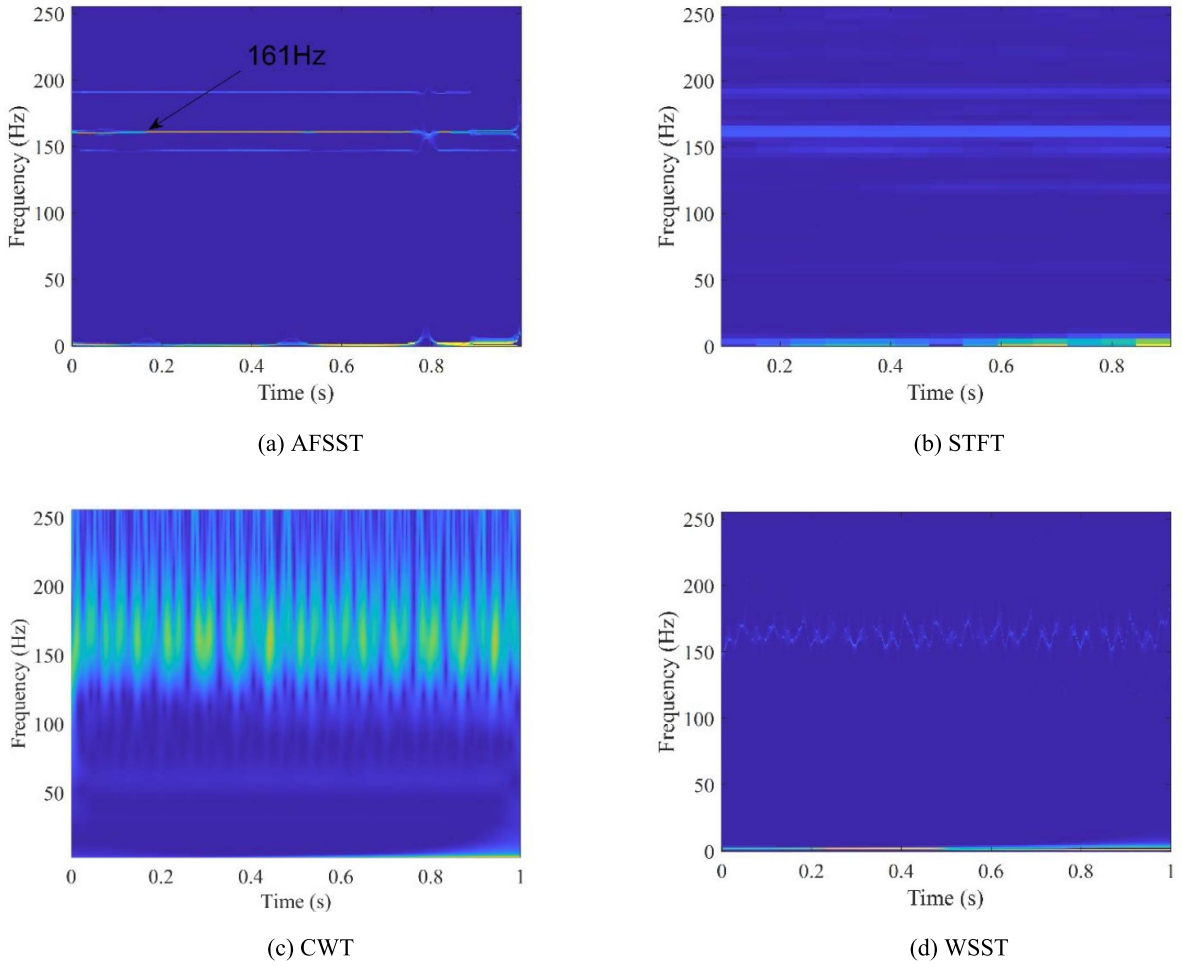

Figure 14. Time-frequency analysis.

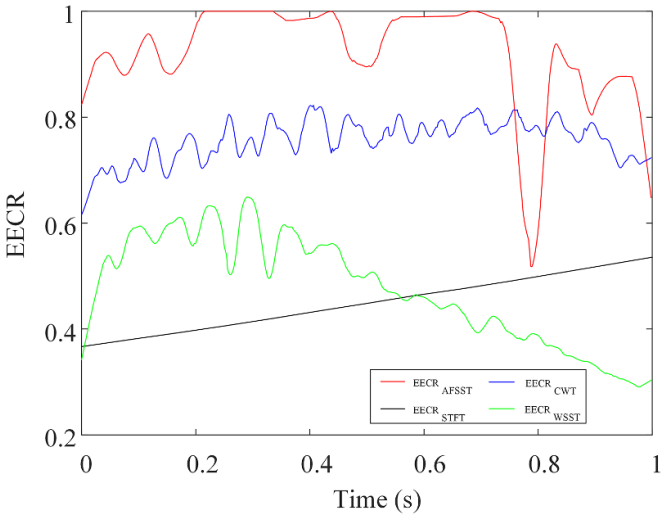

Figure 15. EECR.

In order to pick up and collect vibration signals accurately and quickly, and ensure that the collected vibration data will not be distorted, and can truthfully reflect the vibration of the workpiece, the MDR80 mobile data acquisition, and recording system is selected. The MDR80 mobile data acquisition and recording system can record various types of digital and analog signals, and is widely used in various experimental fields that require dynamic monitoring, such as aerospace engine test runs, aircraft test flight experiments, and automobile experiments. The working condition is set to zero load condition, the bearing rotation frequency is 46 Hz, and the sampling frequency is 20 kHz. The cylindrical roller bearing is selected as the experimental object, as shown in figure 22. Grooves were machined in the bearing inner ring to simulate surface damage failures in actual operation conditions, see figure 23.

The specific bearing parameters are shown in table 4. From the calculation formula above, the fault frequency is 309.1 Hz.

The time domain diagram of the collected bearing fault signal is shown in figure 24, and the time-varying parameters are shown in figure 25.

Figure 26 can be obtained by four time-frequency processing methods such as AFSST, STFT, CWT, and WSST. It can be seen that the time-frequency diagram obtained by AFSST extracts clear bearing fault characteristics, and the rotation frequency and fault frequency can be clearly seen. It also has a good separation effect on the modulation frequency

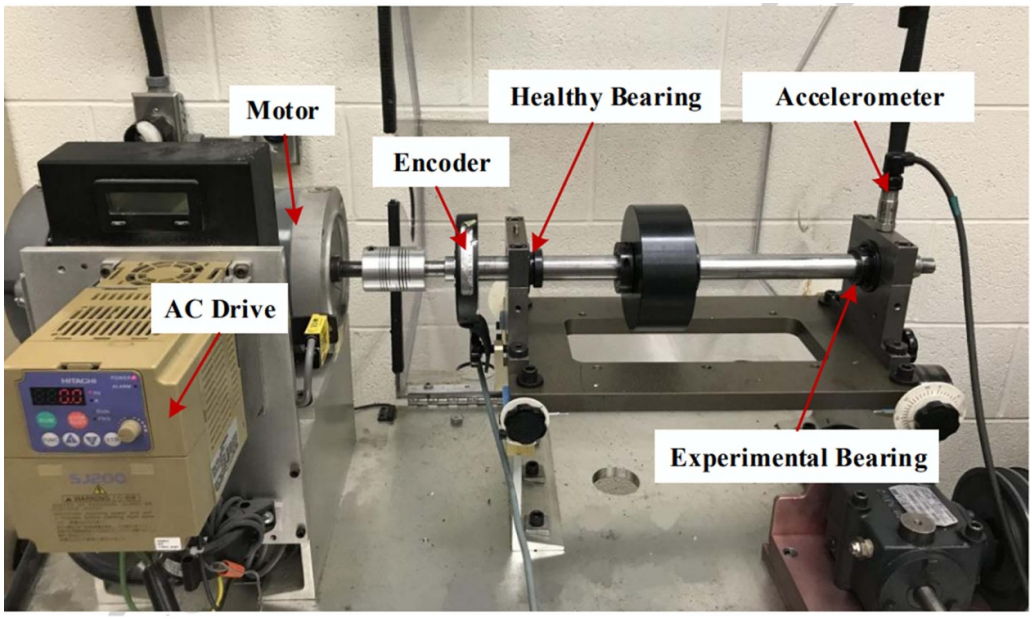

Figure 16. Test bench.

Table 3. Bearing parameters.

Bearing type	Pitch diameter	Roller diameter	Number of the rolling	BPFI	BPFO
ER16K	38.52 mm	7.94 mm	9	$5.43f_r$	$3.57f_r$

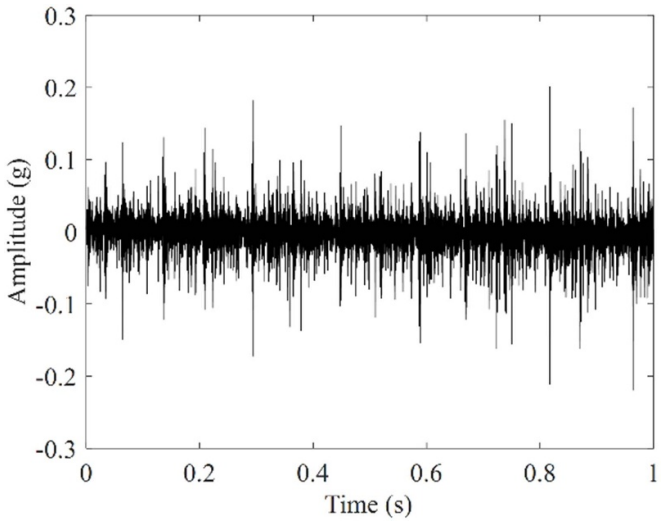

Figure 17. Time domain waveform.

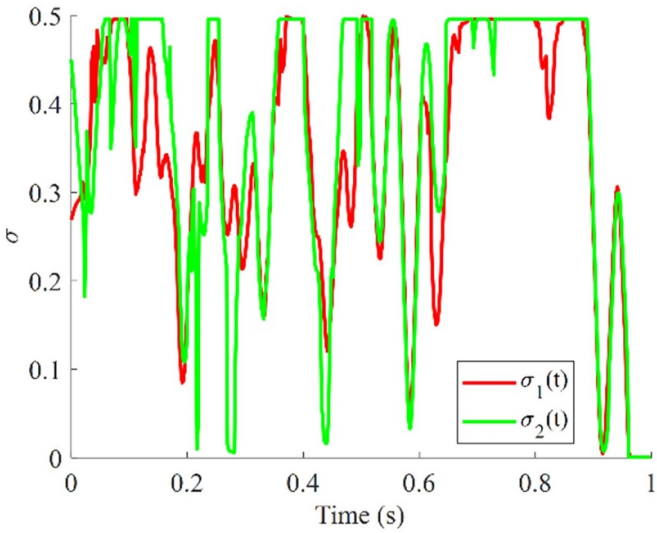

Figure 18. Time parameters.

of the fault feature, and has achieved good frequency resolution and good anti-interference ability in the whole world, which can accurately judge the bearing fault. However, the time-frequency diagrams obtained by methods such as STFT, CWT and WSST can only extract and identify the rotational frequency, which is not ideal for the extraction of bearing fault features, and they all suffer from serious noise interference, so it is difficult to accurately judge the bearing fault state.

Figure 27 shows the EECR parameters proposed in this paper. It can be seen that the AFSST algorithm proposed in this paper has an excellent effective energy accumulation rate

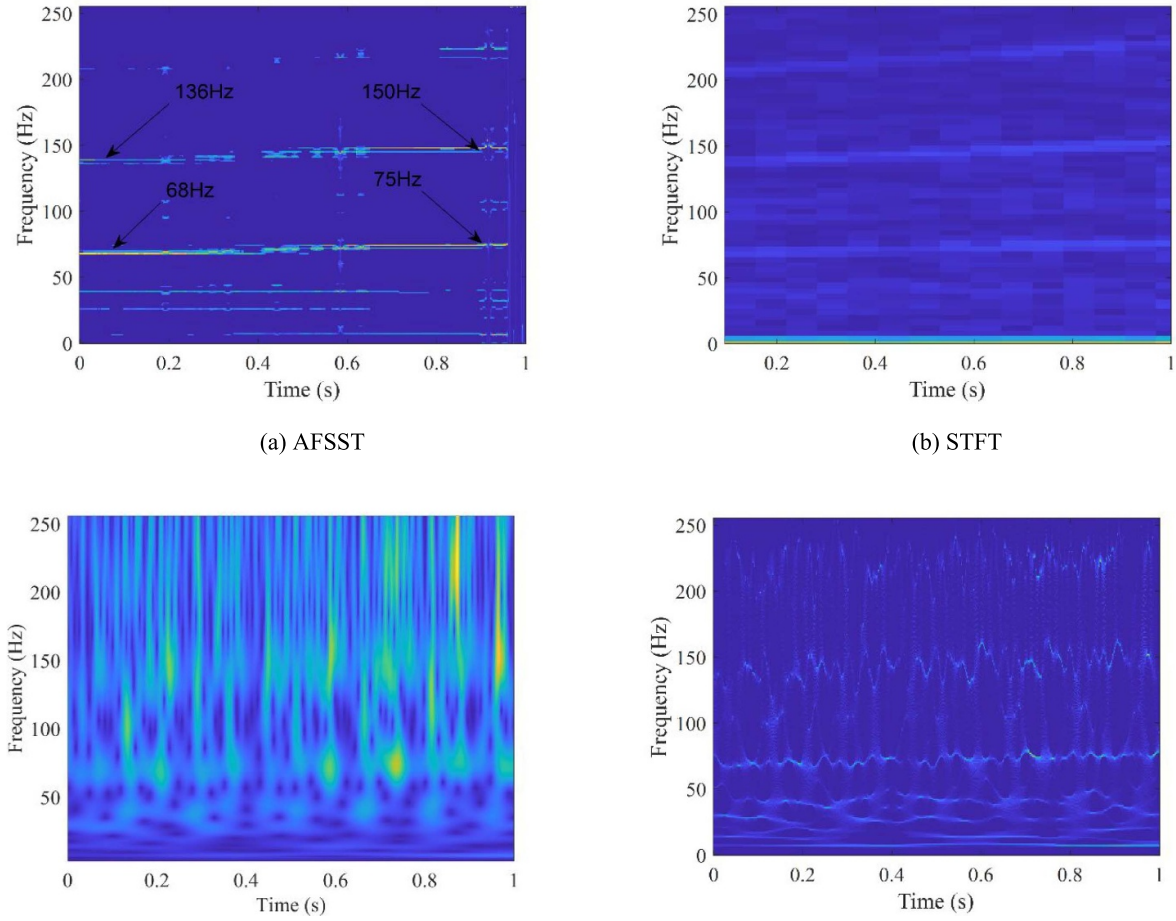

Figure 19. Time-frequency analysis.

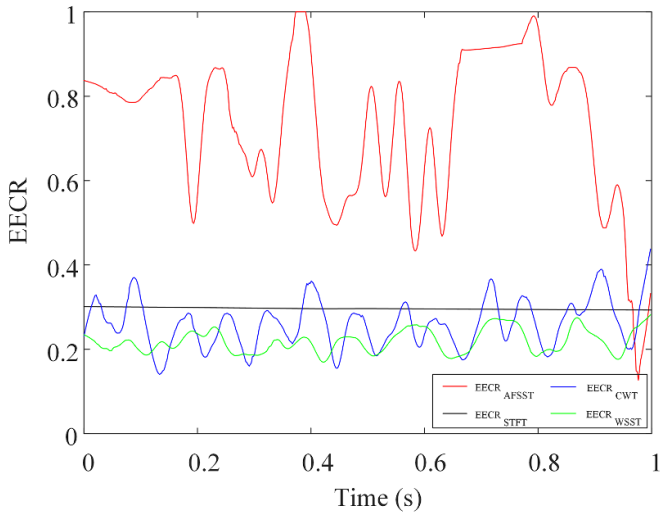

Figure 20. EECR.

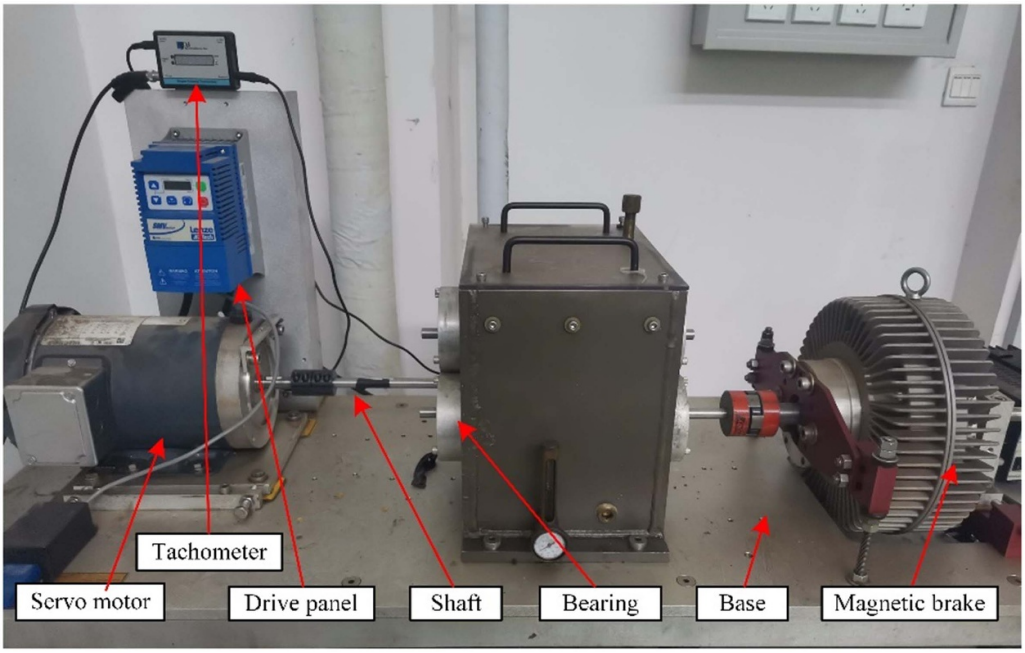

Figure 21. Bearing fault simulation test bench.

Figure 22. Cylindrical roller bearings.

Figure 23. Inner ring fault bearing.

Table 4. Fault bearing parameters.

Bearing type	Outer ring diameter	Inner ring diameter	Roller diameter	Contact angle	Pitch diameter	Number of the rolling
NU 202 ECP	35 mm	15 mm	5.5 mm	0°	24.8 mm	11

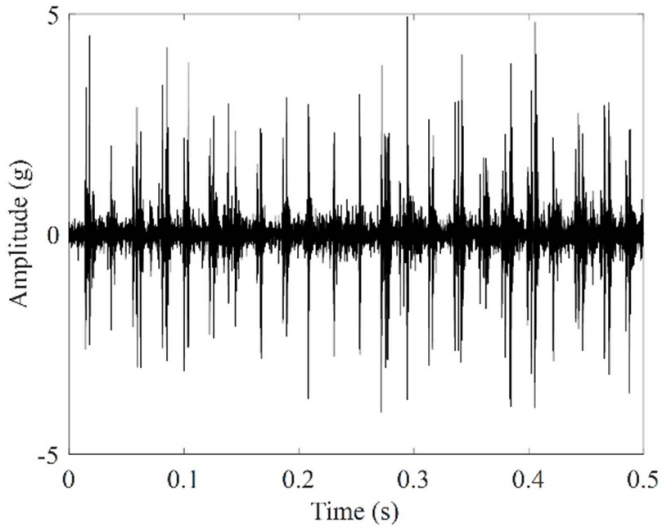

Figure 24. Time domain waveform.

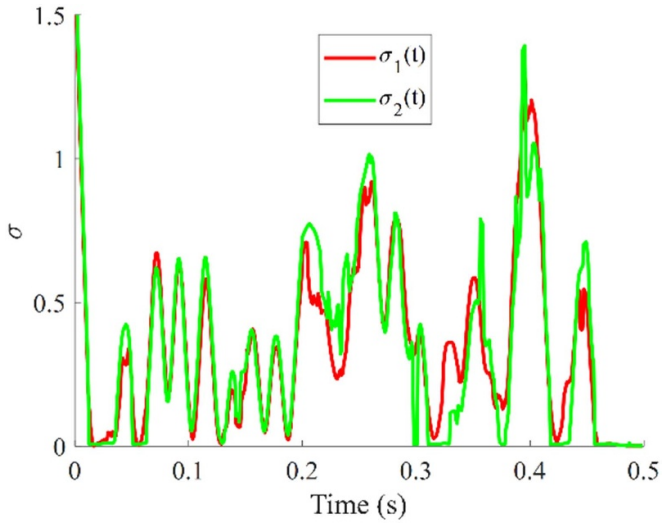

Figure 25. Time parameters.

globally, and has strong fault feature extraction performance and anti-interference performance.

4.4. MFS-MG experimental platform

In order to verify that the method proposed in this paper can achieve better diagnostic results under various working conditions, collect data using the machinery fault simulator – magnum (MFS-MG) mechanical failure comprehensive simulation experiment platform, and the layout is shown in figure 28. A rolling bearing with defects (ER-12K) is installed near the driving motor, and the defects are obtained by electrical discharge machining (EDM), as shown in figure 29. Vibration information is collected by piezoelectric an acceleration sensor. Table 5 shows the basic parameters of rolling bearings.

During the test, the sampling frequency was set as 25.6 kHz and the motor rotation frequency was kept at 29.87 Hz. According to equation (18), the fault frequency is 147.86 Hz. The time-domain diagram of the collected bearing fault signal is shown in figure 30, and the time-varying parameters are shown in figure 31.

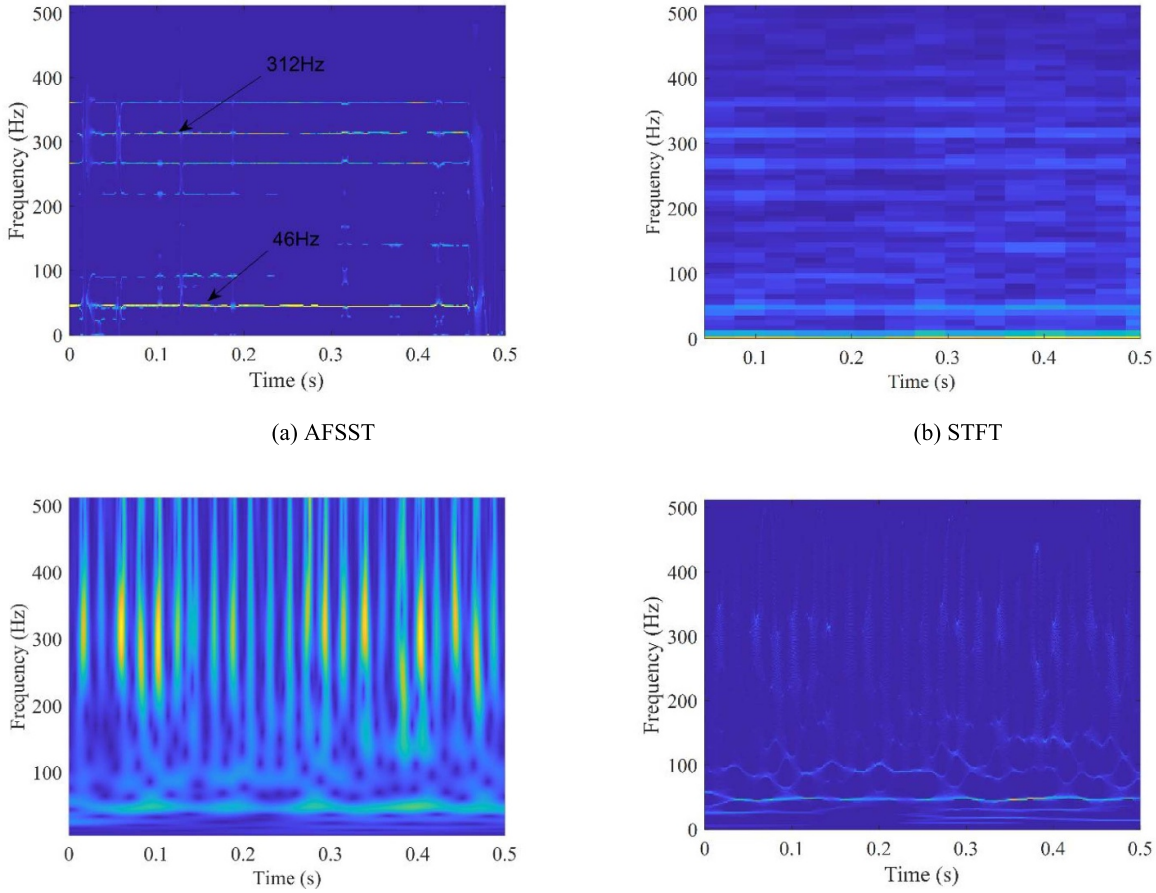

Figure 26. Time-frequency analysis.

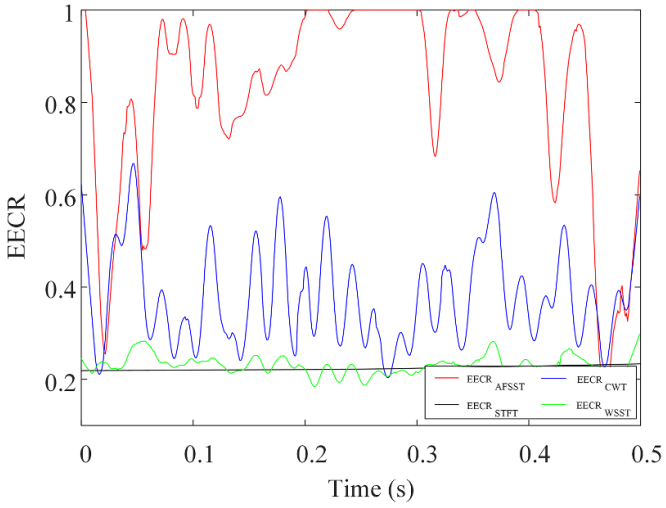

Figure 27. EECR.

Figure 32 can be obtained by four time-frequency processing methods, such as AFSST, STFT, CWT and WSST. The AFSST algorithm can extract clear fault features with a frequency of 148 Hz and its modulation frequency, the rotation frequency is also accurately located, and it also has a strong filtering ability for interference harmonics. However, both STFT and CWT can only see fuzzy characteristic frequency bands, and serious energy diffusion occurs, makes it difficult to determine the core frequency. WSST algorithm can only accurately analyze the rotation frequency, but cannot extract effective fault features. By comparison, it can be proved that the algorithm proposed in this paper has good

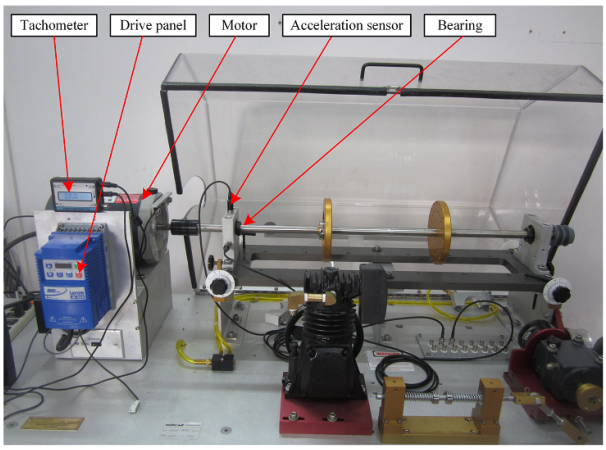

Figure 28. MFS–MG test bench.

Figure 29. Bearing inner ring.

Table 5. Fault bearing parameters.

Bearing type	Outer ring diameter	Inner ring diameter	Roller diameter	Contact angle	Pitch diameter	Number of the rolling
ER-12K	52 mm	25.4 mm	7.93 mm	0°	33.47 mm	8

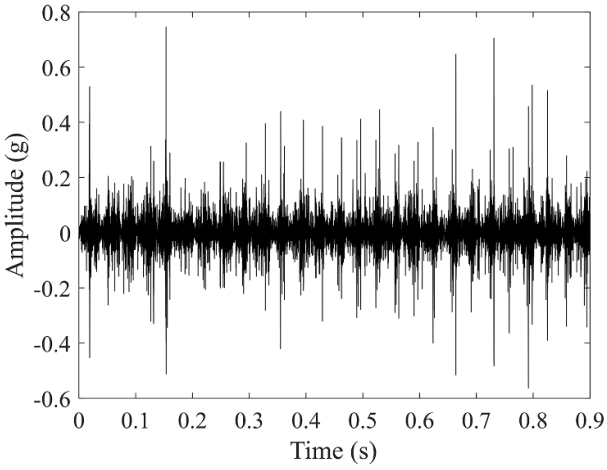

Figure 30. Time domain waveform.

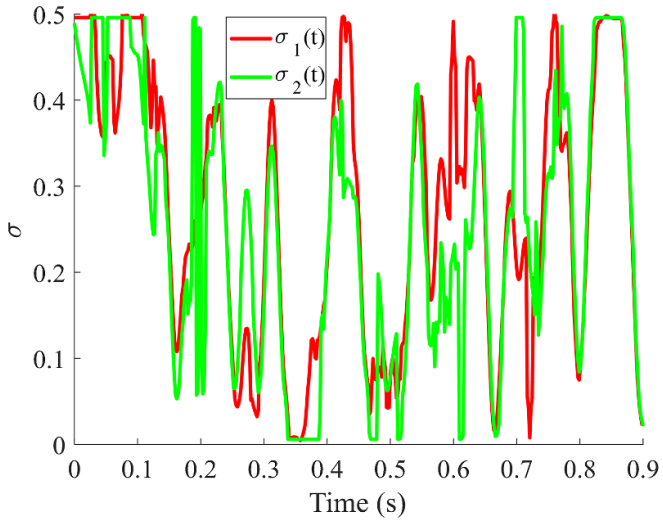

Figure 31. Time parameters.

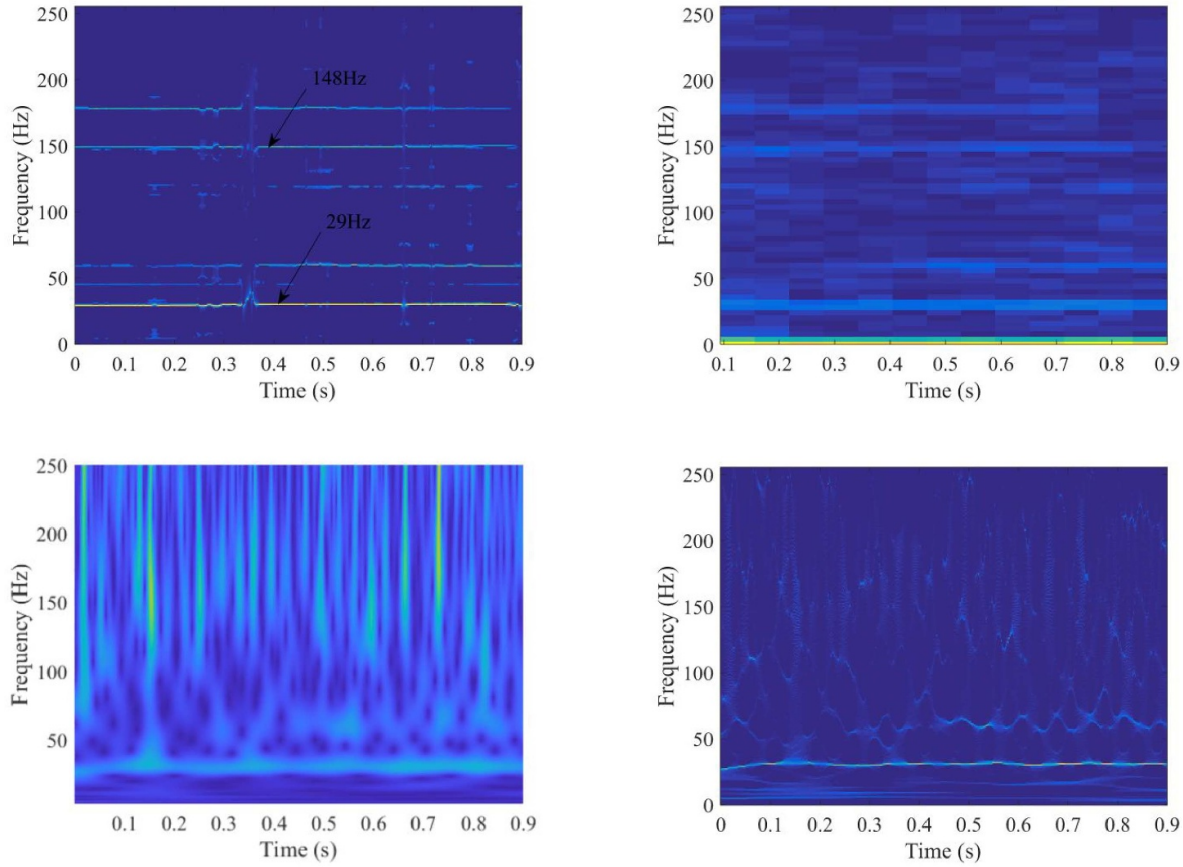

Figure 32. Time-frequency analysis.

feature extraction ability and anti-interference ability, and has strong robustness.

Figure 33 shows the EECR parameters proposed in this paper. It can be seen that the proposed AFSST algorithm has an excellent energy effective compression ratio globally, has strong fault feature extraction performance and anti-interference performance, and can effectively realize bearing fault diagnosis under multiple working conditions.

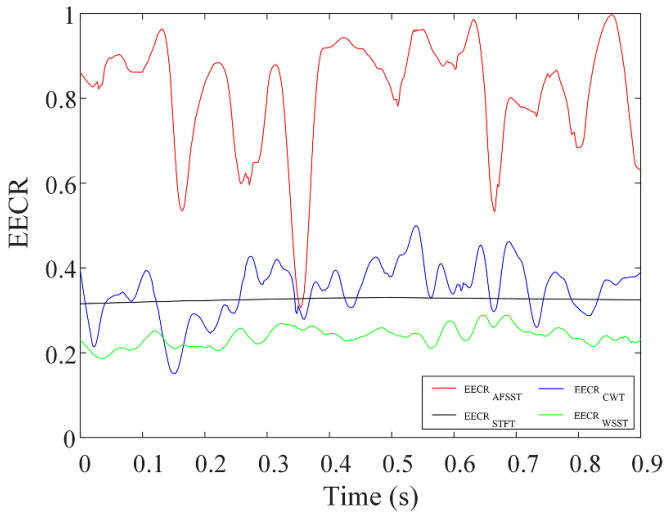

Figure 33. EECR.

5. Conclusion

In this paper, a new time-frequency processing algorithm AFSST based on EMD and FSST is proposed, which improves the adaptability to multi-condition signals, enhances the ability to extract the characteristic frequencies of non-stationary signals, and improves the robustness to noise. Based on good separation conditions, by constructing the time-varying parameter anchor point and introducing the weighted least squares fitting calculation, the time-varying parameter prediction algorithm is established. Through experimental verification, the calculation speed of the time-varying parameter is increased by 29%, and the overall calculation efficiency of AFSST is improved. The EECR parameter is proposed to measure the effective energy aggregation effect and feature extraction ability of the time-frequency analysis method.

Using the simulation signal, the bearing data of Western Reserve University, University of Ottawa variable speed bearing data, and the data collected by the self-built experimental bench, the AFSST, STFT, CWT and WSST processing methods are used for time-frequency processing. Through comparative analysis, it is verified that the AFSST algorithm has great advantages in dealing with non-stationary signals, has strong self-adaptation and can obtain better fault feature extraction results for bearing fault data under different working conditions. This provides a basis for the identification of fault characteristics and has certain application value in practical engineering.

Data availability statement

The data that support the findings of this study were obtained with the support of the Beijing Education Commission. Restrictions apply to the availability of these data, which were used under license for this study.

Author contributions

All authors conceived and designed the study. Software and paper writing, M W; methodology, J Y; supervision, D Y; visualization, J W; data curation, Z H. All authors have read and agreed to the published version of the manuscript.

Conflict of interest

The authors declare no conflict of interest.

Funding

This research was funded by the National Natural Science Foundation of China (51975038), the Nature Science Foundation of Beijing, China (19L00001), the Support plan for the construction of high-level teachers in Beijing municipal universities (CIT&TCD201904062), the Beijing Natural Science Foundation (3214042), the key project of 2020 Science and Technology Plan of Beijing Municipal Commission of Education under Grant (KZ202010016025), and the Beijing Natural Science Foundation Project (L211008).

ORCID iDs

Minghui Wei https://orcid.org/0000-0002-9461-2061
Dechen Yao https://orcid.org/0000-0002-9489-7984

References

[1] Yan G X, Chen J, Bai Y, Yu C Q and Yu C M 2022 A survey on fault diagnosis approaches for rolling bearings of railway vehicles *Processes* **10** 23
[2] Villalba R T, Ramirez H M and Estrada H A 2021 Classification of design methodologies to minimize vibrations in gears and bearings in the 21st century: a review *Machines* **9** 18
[3] Yang J H, Yang C, Zhuang X Z, Liu H G and Wang Z L 2022 Unknown bearing fault diagnosis under time-varying speed conditions and strong noise background *Nonlinear Dyn.* **107** 2177–93
[4] Hua Z H, Shi J J, Jiang X X, Luo Y and Zhu Z K 2021 Matching and reassignment based time-frequency enhancement for rotating machinery fault diagnosis under nonstationary speed operations *Meas. Sci. Technol.* **32** 20
[5] Zhang D and Feng Z P 2022 Enhancement of time-frequency post-processing readability for nonstationary signal analysis of rotating machinery: principle and validation *Mech. Syst. Signal Process.* **163** 28
[6] Choudhury M D, Blincoe K and Dhupia J S 2021 An overview of fault diagnosis of industrial machines operating under variable speeds *Acoust. Aust.* **49** 229–38
[7] Tang G, Wang Y T, Huang Y J and Wang H 2021 Multiple time-frequency curve classification for tacho-less and resampling-less compound bearing fault detection under time-varying speed conditions *IEEE Sens. J.* **21** 5091–101
[8] Tiwari P and Upadhyay S H 2021 Novel self-adaptive vibration signal analysis: concealed component decomposition and its application in bearing fault diagnosis *J. Sound Vib.* **502** 44

[9] Wei S, Wang D, Wang H and Peng Z K 2021 Time-varying envelope filtering for exhibiting space bearing cage fault features *IEEE Trans. Instrum. Meas.* **70** 13
[10] Xu Q S, Liu J B, Guan Y, Sun D Y and Meng Z 2021 Match-extracting chirplet transform with application to bearing fault diagnosis *IEEE Trans. Instrum. Meas.* **70** 10
[11] Chen Z Q, Guo L, Gao H L, Yu Y X, Wu W X, You Z C and Dong X 2021 A fault pulse extraction and feature enhancement method for bearing fault diagnosis *Measurement* **182** 19
[12] Shi J J, Hua Z H, Huang W G, Dumond P, Shen C Q and Zhu Z K 2022 Instantaneous frequency synchronized generalized stepwise demodulation transform for bearing fault diagnosis *IEEE Trans. Instrum. Meas.* **71** 15
[13] Yu G 2021 A multisynchrosqueezing-based high-resolution time-frequency analysis tool for the analysis of non-stationary signals *J. Sound Vib.* **492** 24
[14] Liu Q, Wang Y X and Xu Y G 2021 Synchrosqueezing extracting transform and its application in bearing fault diagnosis under non-stationary conditions *Measurement* **173** 13
[15] Ma Y C, Wang C D, Yang D C and Wang C 2021 Adaptive extraction method based on time-frequency images for fault diagnosis in rolling bearings of motor *Math. Probl. Eng.* **2021** 12
[16] Hu Z, Yang J, Yao D, Wang J and Bai Y 2021 Subway gearbox fault diagnosis algorithm based on adaptive spline impact suppression *Entropy* **23** 660
[17] Xu Y G, Wang L, Yu G and Wang Y X 2022 Generalized S-synchroextracting transform for fault diagnosis in rolling bearing *IEEE Trans. Instrum. Meas.* **71** 14
[18] Jinhai W, Jianwei Y, Yuzhu W, Yongliang B, Tieling Z and Dechen Y 2022 Ensemble decision approach with dislocated time–frequency representation and pre-trained CNN for fault diagnosis of railway vehicle gearboxes under variable conditions *Int. J. Rail Transp.* 19
[19] He Z Y, Shao H D, Ding Z Y, Jiang H K and Cheng J S 2022 Modified deep autoencoder driven by multisource parameters for fault transfer prognosis of aeroengine *IEEE Trans. Ind. Electron.* **69** 845–55
[20] Han B, Li C S, Zhou Y Q, Yu G and Wei C L 2022 Second-order multisynchrosqueezing wavelet transform for bearing fault detection *J. Vib. Eng. Technol.* **10** 1541–59
[21] Shao H D, Li W, Xia M, Zhang Y, Shen C Q, Williams D, Kennedy A and de Silva C W 2021 Fault diagnosis of a rotor-bearing system under variable rotating speeds using two-stage parameter transfer and infrared thermal images *IEEE Trans. Instrum. Meas.* **70** 11
[22] Lee D H, Hong C, Jeong W B and Ahn S 2021 Time-frequency envelope analysis for fault detection of rotating machinery signals with impulsive noise *Appl. Sci.* **11** 16
[23] Zhiyi H, Haidong S, Lin J, Junsheng C and Yu Y 2020 Transfer fault diagnosis of bearing installed in different machines using enhanced deep auto-encoder *Measurement* **152** 107393
[24] Li X, Cheng J, Shao H, Liu K and Cai B 2022 A fusion CWSMM-based framework for rotating machinery fault diagnosis under strong interference and imbalanced case *IEEE Trans. Ind. Inform.* **18** 5180–9
[25] Deng F Y, Liu C, Liu Y Q and Hao R J 2021 A hybrid SVD-based denoising and self-adaptive TMSST for high-speed train axle bearing fault detection *Sensors* **21** 23
[26] Lv Y, Lv S T, Yuan R and Li H W X 2021 Longitudinal synchroextracting transform: a useful tool for characterizing signals with strong frequency modulation and application to machine fault diagnosis *Measurement* **182** 19
[27] Lin R Y, Liu Z W and Jin Y L 2021 Instantaneous frequency estimation for wheelset bearings weak fault signals using second-order synchrosqueezing S-transform with optimally weighted sliding window *ISA Trans.* **115** 218–33
[28] Meng D B, Wang H T, Yang S Y, Lv Z Y, Hu Z G and Wang Z H 2022 Fault analysis of wind power rolling bearing based on EMD feature extraction *CMES-Comput. Model. Eng. Sci.* **130** 543–58
[29] Bai Y, Yang J, Wang J, Zhao Y and Li Q 2021 Image representation of vibration signals and its application in intelligent compound fault diagnosis in railway vehicle wheelset-axlebox assemblies *Mech. Syst. Signal Process.* **152** 107421
[30] Li L, Cai H, Han H, Jiang Q and Ji H 2020 Adaptive short-time Fourier transform and synchrosqueezing transform for non-stationary signal separation *Signal Process.* **166** 15
[31] Liu Z Z, Ding K, Lin H B, He G L, Du C Y and Chen Z Y 2022 A novel impact feature extraction method based on EMD and sparse decomposition for gear local fault diagnosis *Machines* **10** 20
[32] Smith W A and Randall R B Rolling element bearing diagnostics using the Case Western Reserve University data: A benchmark study *Mech. Syst. Signal Process* **64–65** 100–31
[33] Huang H, Baddour N and Liang M 2018 Bearing fault diagnosis under unknown time-varying rotational speed conditions via multiple time-frequency curve extraction *J. Sound Vib.* **414** 43–60